LAWRENCE
LIVERMORE
NATIONAL
LABORATORY

UCRL-JRNL-218577

Pressure effect on the electronic structure of iron in (Mg,Fe)(Al,Si)O3 perovskite: A combined synchrotron Mössbauer and x-ray emission spectroscopy study up to 100 GPa

J. Li, W. Sturhahn, J. Jackson, V. V. Struzhkin, J. F. Lin, J. Zhao, H. K. Mao, G. Shen

February 1, 2006

Physics and Chemistry Minerals

Disclaimer

Pressure effect on the electronic structure of iron in $(Mg,Fe)(Al,Si)O_3$ perovskite: A combined synchrotron Mössbauer and x-ray emission spectroscopy study up to 100 GPa

J. Li, W. Sturhahn, J. Jackson, V. Struzhkin, J. Lin, J. Zhao, H,-k. Mao, G. Shen

ABSTRACT

We investigated the valence and spin state of iron in an Al-bearing ferromagnesian silicate perovskite sample, $(Mg_{0.88}Fe_{0.09})(Si_{0.94}Al_{0.10})O_3$, at 300 K and up to 100 GPa, using diamond-anvil cells and synchrotron Mössbauer spectroscopy techniques. Under elevated pressures, our Mössbauer time spectra are sufficiently fitted by a "three-doublet" model, which assumes two ferrous (Fe^{2+}) iron types and one ferric (Fe^{3+}) iron type with distinct hyperfine parameters. At pressures above 20 GPa, the fraction of the ferric iron, $Fe^{3+}/\sum Fe$, is about 75% and remains unchanged to the highest pressure, indicating a fixed valence state of iron within this pressure range. Between 20 and 100 GPa, the quadruple splittings of all three iron types do not change with pressure, while the isomer shift between the Fe^{3+} types and the Fe^{2+} type increases continuously with increasing pressure. In conjunction with previous x-ray emission data on the same sample, the unchanging quadruple splittings and increasing isomer shift suggest that Fe^{2+} undergoes a broad spin crossover towards the low-spin state at 100 GPa, while Fe^{3+} remains in the high-spin state. The essentially constant quadruple splittings of Fe^{2+} can also be taken as an indication for strong resistance against further distortion of the local iron environment after initial compression.

INTRODUCTION

Aluminum-bearing ferromagnesian silicate perovskite (hereafter referred to as "Al-PV") is believed to be the most abundant phase in the Earth's interior (e.g. Anderson and Bass 1986; Fiquet et al. 2000; Ito et al. 1998; Jeanloz et al. 1992; Li et al. 2005; Liu 1974). It represents at least one third of the total mass of our planet, more than any other terrestrial phase. Knowledge of the physical and chemical properties of Al-PV under the pressure and temperature conditions of the lower mantle is essential to our understanding of the nature and dynamics of the deep Earth's interior. Theoretical considerations and experimental investigations showed that the valence state and spin state of iron have significant effects on the density, thermal conductivity, electrical conductivity, and element partitioning of its host phases (Badro et al. 2004; Burns 1993; Fei et al. 2005; Katsura et al. 1998; Li et al. 1993; Lin et al. 2005; Sherman 1988; Speziale et al. 2005; Wood and Rubie 1996; Xu et al. 1998). Given its potentially far-reaching consequences, accurate characterization of the electronic structure of iron in Al-PV under lower mantle pressure conditions is necessary for our understanding of the physics and chemistry of the lower mantle.

Many studies have been carried out to investigate the crystal chemistry of Al-free PV (Jackson et al. 2005). Fewer studies are available for Al-PV, including ^{57}Fe Mössbauer spectroscopy at 1 bar (Lauterbach et al. 2000; McCammon 1998), element partitioning (Wood and Rubie 1996), x-ray emission spectroscopy (XES) (Li et al. 2004), single crystal x-ray diffraction (Vanpeteghem et al. 2005), atomistic simulations (Richmond and Brodholt 1998), and transmission electron microscopy (Frost et al. 2004). The XES study revealed a pressure-induced gradual loss of magnetic moment in Al-PV, indicating the occurrence of intermediate-spin state and mixed spin state in Al-PV under high pressures (Li et al. 2004). The change in the spin state of iron takes place over a range of pressure, without any accompanying structural transformation. In this paper, we will use the term "spin crossover" to denote the spin state change in perovskite, in order to emphasize its broad nature (e.g. Jackson et al. 2005; Sturhahn et al. 2005).

Due to possible occurrence of multiple broad spin crossover in Al-PV, the path of spin evolution could not be resolved based on the x-ray emission data alone. Moreover, *in situ* measurements of the valence state of iron in Al-PV have not been performed under high pressures. Mössbauer spectroscopy can provide information on the valence state and spin state of iron. Conventional Mössbauer spectroscopy has been performed to Mbar pressures using diamond anvil cells on samples with relatively high iron contents (Pasternak et al. 1997; Speziale et al. 2005) (Speziale et al. 2005). Recent developments in synchrotron Mössbauer spectroscopy (SMS) have enabled *in situ* measurements of small samples (< 10 μm) with relatively low iron contents (< 10 at.%) to Mbar pressures (Jackson et al. 2005; Sturhahn 2004; Zhang et al. 1999). In Mössbauer spectroscopy each iron type has its characteristic set of hyperfine parameters (Figure 2). By observing type-specific hyperfine parameters, it is possible to monitor changes in the valence state, spin state, and crystallographic site of each iron type. However, the characteristic hyperfine parameters of iron in perovskite at various spin states are not known. While an abrupt spin transition may be readily recognizable from the pressure dependence of isomer shift and quadruple, resolving multiple broad spin crossover using Mössbauer spectroscopy would require detailed modeling of pressure dependence of the electronic density at the nucleus and the electric field gradient. Alternatively, we can combine Mössbauer spectroscopy with x-ray emission spectroscopy, a probe for the local magnetic moment of iron (Rueff et al. 1999; Struzhkin et al. 2000; Tsutsumi et al. 1976), to investigate the pressure effect on the electronic structure of iron in perovskite. In this study, we apply the SMS techniques to the same Al-PV sample that was studied previously using the XES techniques (Li et al. 2004), in order to monitor the valence state of iron as a function of pressure, and to derive new constraints on the spin state evolution of iron in Al-PV under lower mantle pressures.

EXPERIMENTAL METHOD

Synchrotron Mössbauer spectroscopy experiments

Immediately following the x-ray emission study (Li et al. 2004), SMS measurements were carried out at beamline 3-ID of the Advanced Photon Source, Argonne National Laboratory. Four fragments of samples were investigated: Two fragments were glued to a beryllium foil, one fragment loaded into a wide-angle panoramic cell (Mao et al. 2001), and one fragment the same as used in the XES study. In the panoramic cell, two flat diamonds with 600 μm culet size were mounted on carbide seats. A beryllium disc (1mm thick, 5mm in diameter) was pre-indented to 50-μm thickness and drilled to create a 300 μm hole. The hole was filled with amorphous boron and pressed between the two diamonds. A 100 μm hole was drilled into the compressed boron to create a sample chamber, in which a fragment of Al-PV and several ruby grains were loaded. The use of boron gasket helps to strengthen the Be gasket, increase the sample volume, and reduce the pressure gradients across the sample. Ruby was used as a pressure marker (Mao et al. 1986; Zha et al. 2000). In the cell from the XES study, high pressure was generated using a symmetrical piston-cylinder type diamond-anvil cell made by the Geophysical Laboratory. Two beveled diamonds (about 300 micron bevel size and 150 micron culet size) were mounted in the cell. An x-ray transparent beryllium disc (1 mm thick and 5 mm in diameter) was pre-indented to about 20 micron in thickness then drilled to create a 50-micron-sized sample chamber. A piece of Al-PV sample and a few grains of ruby were loaded into the chamber and sandwiched between the two diamonds. Sample pressure was determined from the laser-induced fluorescence spectrum of ruby at GSECARS. Near 100 GPa, the ruby pressures were confirmed by the positions of the Raman peaks of the diamonds.

The details of the SMS measurements are similar to that described in Jackson et al. (Jackson et al. 2005). The electron storage ring was operated in top-up mode with 23 bunches that were separated by 153 ns. The incident x-ray with a bandwidth of 1 meV was tuned to the nuclear transition energy of 14.4125 keV using multiple-crystal Bragg reflection monochromators

(Toellner 2000). It was then focused to a spot size of 6x6 μm^2 at the full-width half-maximum using a Kirkpatric-Baez mirror system (Eng et al. 1998). With a flux of 10^9 photons/second at the focal spot, sufficient counting rate could be obtained on the small sample over a reasonable acquisition time period. Nuclear resonant scattering was observed in a time window of 20 to 120 ns following excitation. Time spectra were collected at 0 GPa on the Al-PV fragment loaded onto a piece of Be foil, at 2 to 30 GPa on the Al-PV fragment loaded in the panoramic cell, and at 100 and 80 GPa on the Al-PV fragment from the XES study.

Evaluation of time spectra

The SMS data were evaluated following the same procedure as described in Jackson et al. (Jackson et al. 2005). The CONUSS software was used for analysis (Sturhahn 2000; Sturhahn and Gerdau 1994). Not always was it possible to vary all parameters simultaneously. This situation is indicated by values without errors. The valence state of iron is associated with specific ranges of the hyperfine parameters derived from the synchrotron Mössbauer data. The distinctly different electric field gradients of Fe^{2+}- and Fe^{3+}-like crystal sites permit us to determine the $Fe^{3+}/\Sigma Fe$ ratio (Table 1). In some cases, the $Fe^{2+}{}_1$ type could not be distinguished as indicated by dashes. The thickness was fixed at about 3 μm ^{57}Fe, equivalent to about 150 μm of the Al-PV fragment measured under ambient conditions. For the fragments in the DACs, we obtain 0.5 μm and 0.3 μm ^{57}Fe, equivalent to about 25 μm and 15μm Al-PV, respectively. The results were insensitive to the exact thickness values. The distribution functions are of Gaussian type, and widths are given at half the maximum of the Gaussian. As no external standard was used, the isomer shift values are given with respect to the $Fe^{2+}{}_2$ type. With the exception of the 100 GPa data, a non-zero isomer shift between the two Fe^{2+} types did not improve the fit quality. The isomer shift between the two Fe^{2+} types was set to zero. At 100 GPa, the isomer shift between the Fe^{2+} types is 0.10(1) mm/s.

RESULTS AND DISCUSSION

The measured and calculated time spectra are shown in Figure 1. At 1 bar, a "two-doublet model" provides a satisfactory fit to the spectrum. Under elevated pressure, a "three-doublet model" is necessary and sufficient to fit the spectra. These doublets are broadened probably due to distributed electric field gradients acting on the ^{57}Fe nuclei. The "three-doublet model" has been applied earlier to explain Mössbauer data on similar $(Fe,Mg)SiO_3$ perovskites at ambient pressure conditions (Fei et al. 1994), and in the high-pressure regime (Jackson et al. 2005). Similar models have also been employed to analyze Mössbauer spectra of $(Fe,Mg)(Al,Si)O_3$ perovskite at ambient pressure conditions (Lauterbach et al. 2000). The fitted parameters for the data set are displayed in Table 1 and Figure 2.

Site occupancy of iron

The valence state and spin state of iron in perovskite are intimately connected to the crystallographic site it occupies. Knowledge on the site occupancy of iron can greatly facilitates the interpretation of Mössbauer and x-ray emission spectra. Conversely, the hyperfine parameters extracted from Mössbauer spectra and the spin state information given by x-ray emission spectra may provide constraints on the site occupancy of iron. Previous x-ray diffraction and spectroscopy measurements have established that Fe^{2+} resides in the 8-12 coordinate site (the A site) in both Al-free and Al-bearing perovskites (Fei et al. 1994; Jackson et al. 1987; Jephcoat et al. 1999; Keppler et al. 1994; Lauterbach et al. 2000; McCammon et al. 1992; Parise et al. 1990; Shen et al. 1994; Vanpeteghem et al. 2005). The site occupancy of Fe^{3+} is poorly constrained and has been shown to be sensitive to Al concentration (Frost and Langenhorst 2002; Hirsch and Shankland 1991; Jackson et al. 2005; Lauterbach et al. 2000; McCammon 1997; McCammon et al. 1992). Earlier studies suggest that Fe^{3+} occupies the octahedral site (the B site) only at low Al concentrations, and it occupies both A and B sites through a coupled substitution: $^{A}Fe^{3+} + {}^{B}Fe^{3+}$ —

$^{A}Mg^{2+}$+ $^{B}Si^{4+}$ when the Al concentration is high. Recent x-ray diffraction data on several single-crystal Al-free and Al-PV samples show that all the iron take the A site (Vanpeteghem et al. 2005). Our sample does not contain a large enough single crystal for direct determination of site occupancy using x-ray diffraction techniques. Powder x-ray diffraction spectra were acquired using both laboratory and synchrotron radiation source but the data did not allow assignment of crystallographic site for iron. The sample contains comparable amounts of Fe^{3+} and Al^{3+}. Since the smaller trivalent cation Al^{3+} preferentially occupies the smaller B site, ferric iron is likely to occupy the A site through a coupled substitution: $^{A}Fe^{3+} + {}^{B}Al^{3+}$ — $^{A}Mg^{2+}$+ $^{B}Si^{4+}$. Additional indications for the ferric iron occupying the A site of the Al-PV come from its quadruple splitting, which is larger and less broadened (expressed as FWHM in Table 1 and as the uncertainty on QS in Figure 2) than that of Al-free perovskite (Jackson et al. 2005): the distortion of the A site leads to a larger quadruple splitting, while the single site occupancy gives rise to less broadening. In the following discussion, we will assume that both Fe^{2+} and Fe^{3+} are in the A site.

Pressure effect on the valence state of iron

Basic properties of the lower mantle, including major element distribution and electrical conductivity, depend critically on the valence state of iron in the predominant phase perovskite (Katsura et al. 1998; Li et al. 1993; Wood and Rubie 1996; Xu et al. 1998). Pressure-induced valence state changes have been reported previously. Drickamer and coworkers observed reduction of ferric to ferrous iron under high pressure, probably due to charge transfer from ligand to metal (Champion et al. 1967). The reverse reaction, i.e. oxidation of ferrous to ferric iron, occurs in $Fe(OH)_2$ and was attributed to pressure-induced deformation of OH dipole (Pasternak et al. 2004). A third type of redox reaction, in which ferric iron decomposes to form ferric iron and iron metal at high pressure and high temperature, has been proposed to account for the ferric iron in perovskite samples synthesized from ferric-iron-free orthopyroxene starting materials (Fei et al. 1994; Frost et al. 2004; Lauterbach et al. 2000; Li et al. 2004; McCammon 1997; McCammon et al. 2004; McCammon 1998). On the other hand, recent synchrotron Mössbauer spectroscopy study found that pressure alone does not alter the valence state of iron in Al-free perovskite (Jackson et al. 2005).

In our Al-PV, the fraction of ferric iron, $Fe^{3+}/\sum Fe$, is about 50% at ambient conditions (Table 1 and Figure 2). During initial compression to 12 GPa, the fraction of ferric iron barely changes. Between 12 and 20 GPa, the fraction of Fe^{3+} increases drastically to 75%, mainly at the expense of $Fe^{2+}{}_1$. At pressures above 20 GPa, the fraction of ferric iron remains essentially constant again up to the highest pressure of our experiments. The abrupt changes occur at pressures comparable to the observed spin transition in iron metal (Rueff et al. 1999). We tried to fit the abrupt change by assuming that the starting material contains a small amount of iron metal but it didn't work. A simple charge balance calculation for iron gives an average charge of +2.5 at pressures below 12 GPa and +2.75 at pressures above 20 GPa. To account for the apparent increase in the average charge of iron by a redox reaction, half of the ferrous iron would have become ferric. At ambient conditions, the volume of the Al-PV sample is at least half of that of oxygen in the air that is trapped in the sample chamber (including the air trapped between Al-PV grains). The density of Al-PV is about four thousand times that of air. Although the iron content of the Al-PV is very low, the amount of O that is needed to oxidize half of the Fe^{2+} into Fe^{3+} is at least four times of the amount of free O in the sample chamber. Hence the increase in the fraction of Fe^{3+} between 10 and 20 GPa cannot be explained by an oxidation reaction. Because the mysterious change of valence state occurs outside the stability field of Al-PV and is not directly relevant to the Earth's lower mantle, we will not discuss it further. Between 20 and 100 GPa, the essentially constant fraction of ferric iron indicates that pressure alone does not alter the valence state of iron in the Al-PV within this pressure range.

Pressure-induced spin crossover

One of the important parameters for geophysical model of the lower mantle is the spin state of iron, as it can influence the density, thermal conductivity, and element partitioning of the host phases (Badro et al. 2004; Burns 1993; Fei et al. 2005; Li et al. 2004; Li et al. 2005; Lin et al. 2005; Sherman 1988). Although structurally stable to a depth that is greater than 2000 km, pressure-induced changes in the electronic spin state of iron have been observed in both Al-PV and Al-free perovskites within the lower mantle pressure range (Badro et al. 2004; Jackson et al. 2005; Li et al. 2004). Unlike well-known examples of spin transitions in pure Fe and FeS (e.g. Rueff et al. 1999), which are abrupt changes in the spin state accompanied by structural phase transitions, the loss of magnetic moment in perovskites occurs gradually with increasing pressure (Jackson et al. 2005; Li et al. 2004). There were indications for intermediate-spin state in perovskite, as expected for the relatively low site symmetry for iron and variable degree of distortion in the A site (Li et al. 2004). Under given pressure and temperature conditions, iron with different valence states and/or crystallographic site occupancy may have different spin states, leading to a mixed spin state in perovskite (Li et al. 2004). The iron content of lower mantle perovskites is less than 10 at.%, even if we assume all of the iron goes into perovskites. At such a low concentration level, a change of spin state is likely to spread over a wide pressure-temperature range (Li et al. 2005; Sturhahn et al. 2005). In x-ray emission spectroscopy, the intensity ratio between the Kβ' satellite peak and the $K\beta_{1,3}$ main peak reflects the number of unpaired electrons in the 3d sub-shell, which is determined by the valence state and spin state of iron (Figure 3). Possible spin configurations can be deduced from a comparison between the calculated intensity ratios and observed values. Between 20 and 100 GPa, the XES intensity ratio decreases continuously with increasing pressure, indicating one or more gradual spin crossover towards lower spin states. The intensity ratio at 100 GPa can be matched by several spin configurations, including 1) Fe^{2+} in the high-spin state and Fe^{3+} in the low-spin state, 2) Fe^{2+} in the low-spin state and Fe^{3+} in the high-spin state, 3) Fe^{2+} in the intermediate-spin state and Fe^{3+} in the low-spin state, and 4) Fe^{2+} in the low-spin state and Fe^{3+} in the intermediate-spin state. In the following discussion, we will refer to these configurations as 2H3L, 2L3H, 2M3L, and 2L3M, respectively. From the x-ray emission data alone, these configurations cannot be distinguished, and the path of pressure-induced spin crossover in Al-PV cannot be determined.

Complimentary information on the spin evolution of iron may be derived from the new SMS data on the same sample. Although the characteristic hyperfine parameters of iron at various spin states are barely known for oxides and silicates, the effect of pressure-induced spin crossover on the isomer shift and quadruple splitting can be assessed qualitatively based on the principles of Mössbauer effect (Bancroft 1973; Wertheim 1964). The QS of iron is determined by the electric field gradient at the nucleus, and can be regarded as a combination of contributions from valence electrons and from the rest of the crystal lattice, including site distortion and next-nearest neighbor environment (Bancroft 1973; McCammon 1998). For high-spin Fe^{3+}, the valence contribution is zero because all five 3d orbitals are equally populated, leading to a highly symmetric electron configuration. At lower spin states, the electronic configurations are less symmetric, hence the valence contribution should be non-zero. Indeed, the low-spin Fe^{3+} in Fe_2O_3 has a relative large QS (2 mm/s at 82 GPa) (Pasternak et al. 1999). For Fe^{2+} in the A site, a spin crossover in Fe^{2+} may not have any detectable effect on the QS because the electronic configurations at various spin states are similarly asymmetric. Between 20 and 100 GPa, the QS of all three iron types remain essentially constant (Figure 2). Given the insensitivity of the QS of Fe^{3+} to lattice distortion (Burns and Solberg 1990), the constant QS of Fe^{3+} does not support a pressure-induced spin reduction in Fe^{3+}, which would have led to the 2H3L, 2M3L, or 2L3M state at 100 GPa. Considering that the QS of Fe^{2+} in the A site is not sensitive to its spin state, the constant QS of Fe^{2+} is consistent with a pressure-induced spin reduction in Fe^{2+}. The IS of iron is determined by the electronic density at its nucleus. With decreasing ionic radius, the electronic

density increases, and the IS decreases. Iron at a lower spin state is expected to have a smaller ionic radius (Burns 1993; Shannon and Prewitt 1969), hence a smaller IS. In our experiments, the IS between Fe^{3+} and Fe^{2+} increases with pressure and approaches zero at 100 GPa (Figure 2), which is consistent with a pressure-induced spin crossover in Fe^{2+} leading to the 2L3H state at 100 GPa, but does not support a pressure-induced spin crossover in Fe^{3+} leading to the 2L3H state at 100 GPa. Thus, in conjunction with the previous XES results, our SMS data suggest that Fe^{2+} undergoes a spin crossover between 20 and 100 GPa while Fe^{3+} stays in the high-spin state. This result is also consistent with the inferred occupancy of both Fe^{2+} and Fe^{3+} in the A site: with a larger ionic radius, Fe^{2+} experiences a higher "chemical" pressure and is likely to transform to the low-spin state at lower pressure than Fe^{2+}.

Lattice distortion

The presence of two Fe^{2+} types has been observed in Al-free PV and Al-PV at ambient conditions and was interpreted as a reflection of varying degrees of distortion at the A site (Fei et al. 1994; Lauterbach et al. 2000; McCammon 1998). In Al-PV, different surrounding cation configurations could be a cause for varying degrees of distortion (e.g. Li et al. 2005). X-ray diffraction studies show that perovskite is elastically anisotropic and becomes distorted under pressure (Andrault et al. 2001; Fiquet et al. 2000; Mao et al. 1991). If site distortion is the origin of the two Fe^{2+} types, the appearance of the second Fe^{2+} type with a larger QS under elevated pressure would indicate that a fraction of the A sites become significantly more distorted upon compression (Figure 2). Accompanying the abrupt increase in the fraction of Fe^{3+} between 12 and 20 GPa, the QS of Fe^{3+} broadens significantly (Table 1 and Figure 2), probably because the next-nearest neighbor environment of the newly produced Fe^{3+} differ from that in the starting material. Above 20 GPa, the QS values of all three iron types remain essentially constant. Because the QS of Fe^{2+} in the A site is not sensitive to its spin state, the unchanging QS values of Fe^{2+} can be taken as an indication for strong resistance against further distortion of the local iron environment after initial compression.

CONCLUSIONS

In this study, we show that the combination of SMS and XES techniques can provide new insight into the path of multiple broad spin crossover in Al-PV, which is not resolvable by SMS or XES alone. Considering the broadening effect of temperature on spin crossover in lower mantle minerals (Sturhahn et al. 2005), such combination would be particularly useful for investigating the valence and spin state of iron at simultaneous high pressure and high temperature that are prevalent in the Earth's interior. The measured hyperfine parameters can be used to test and refine theoretical modeling of the electronic structure of iron in lower mantle perovskite. The new constraints on the valence and spin state of iron in Al-PV will contribute to our understanding of the density, transport properties and element partitioning in the Earth's deep interior.

ACKNOWLEDGEMENT

We thank Ross Angel at Virginia Tech for insightful discussion on the site occupancy of iron in perovskites, and for trying to perform a single-crystal x-ray diffraction measurement on our Al-PV sample. We thank Holger Hellwig at U. Illinois for providing helpful comments and suggestions on the earlier drafts of the paper. We thank Jinfu Shu at the Geophysical Laboratory for helping with gasket preparation. This work is supported by NSF grant. This work at LLNL was performed under the auspices of the U.S. DOE by University of California and LLNL under Contract No. W-7405-Eng-48. J.F.L. is also supported by Lawrence Livermore Fellowship.

Table 1. The best-fit parameters from Mössbauer spectroscopy measurements

P (GPa)	Fe^{2+}_1 fraction	QS (mm/s)	FWHM (mm/s)	Fe^{2+}_2 fraction	QS (mm/s)	FWHM (mm/s)	Fe^{3+} fraction	QS (mm/s)	FWHM (mm/s)	IS (mm/s)
SMS fragment 1										
0	-	-	-	0.46(1)	2.11(1)	0.70(1)	0.54	0.77(1)	0.31(1)	-0.70(1)
SMS fragment 2, wide-angle DAC										
3	-	-	-	0.47(1)	2.09(1)	1.19(1)	0.53	0.90(1)	0.48(1)	-0.42(1)
12	0.07(1)	2.40(1)	1.05	0.40(1)	2.20(1)	1.29(1)	0.53	0.89(1)	0.60(1)	-0.32(1)
20	0.09(1)	3.49(1)	0.35	0.13(1)	2.65(1)	0.26	0.78	0.89(1)	0.83(1)	-0.20(1)
30	0.10(1)	3.55(1)	0.36	0.15(1)	2.75(1)	0.27(1)	0.75	0.88(1)	0.81(1)	-0.21(1)
SMS fragment 3, DAC "009"										
80	0.11(1)	3.47(1)	0.04	0.15(1)	2.55(4)	0.14(5)	0.74	0.81(2)	0.74(9)	-0.14(3)
100	0.11(1)	3.45(1)	0.03	0.15(1)	2.60(1)	0.08	0.74	0.80(2)	0.75(3)	-0.06(1)

Notes: QS - quadruple splitting, FWHM- full width at half maximum of the QS, IS - isomer shift between Fe^{3+} and Fe^{2+}; Conventional Mössbauer measurements found that IS(Fe^{3+}) = 0.43, IS(Fe^{2+}) = 1.12, with respect to alpha iron; Numbers in parenthesis are the uncertainties on the last reported digit, based on the 2σ of the fitted parameters.

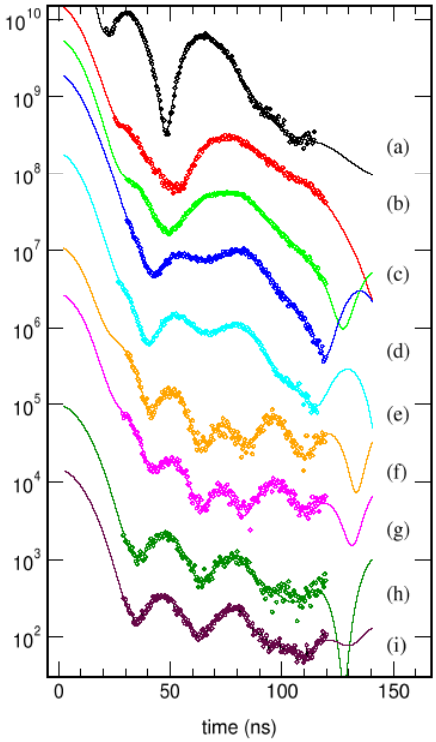

Fig. 1. SMS time spectra (filled circles) and calculates with best-fit parameters given in Table 1 (solid lines) at the following pressures: (a) ambient (b) 12 GPa, (c) 20 GPa, (d) 30 GPa, (e) 80 GPa, (f) 100 GPa. The spectra are offset for clarity.

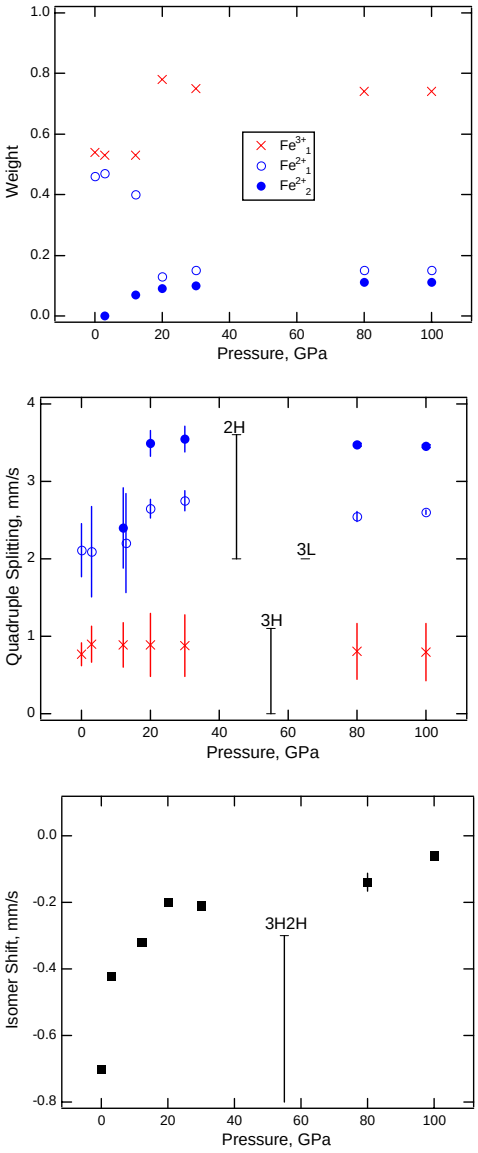

Fig. 2. (a) Fractions of the three modeled iron types as obtained from fits of the time spectra, **(b)** Quadruple splittings derived from time spectra. The size of the bars gives the FWHM of the Gaussian broadening. Symbols at 12 GPa are horizontally offset by 1 GPa for visibility. The ranges of quadruple splittings for high-spin Fe^{2+} (2H) and high-spin Fe^{3+} (3H), as determined by conventional Mössbauer spectroscopy (Bancroft 1973), and one value for low-sin Fe^{3+} (3L) (Pasternak et al. 1999) are shown for references. **(c)** Isomer shift of the Fe^{3+} type relative to the Fe^{2+} types from fits of the time spectra. The range of isomer shift between 2H and 2H, as determined by conventional Mössbauer spectroscopy (Bancroft 1973) are shown for references. The lower end of the ranges extend beyond the scale of the plot.

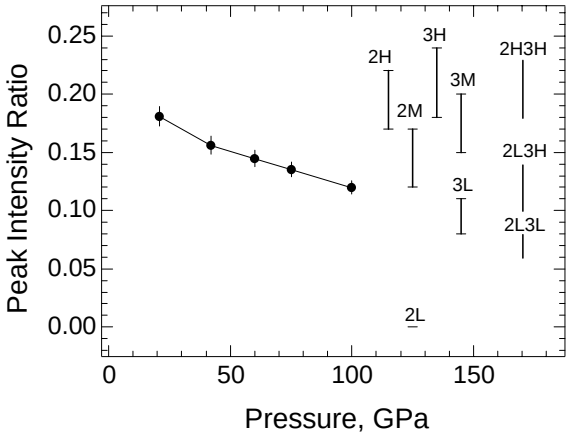

Fig. 3. Comparison between the observed and calculated intensity ratios between the Kβ' satellite peak at about 7.045 KeV (I') and the $K\beta_{1,3}$ main peak at about 7.058 KeV (I) in x-ray emission spectra. Solid circles with error bars are experimental data (Li et al. 2004). Vertical lines and a bar shows the ranges or value of intensity ratios calculated for various iron types, denoted by its valence state (2 = Fe^{2+}, 3 = Fe^{3+}) and spin state (H = high-spin, M = intermediate-spin, L = low-spin). The intensity ratio for each iron type is calculated according to I'/I = N/(N+2)/c, where N is the number of unpaired electrons in the incomplete 3d shell of iron, c is an empirical correction factor with a value between 3 and 4 (Tsutsumi et al. 1976). Dashed lines indicates the ranges of intensity ratios calculated for three possible spin configurations of iron in Al-PV, by summing up contributions from all iron types according to $I'/I = \sum(f_i \bullet N_i/(N_i+2))/c$, where the subscript "i" refers to a specific iron type, f_i refers the fraction of i, N_i refers to the number of unpaired electrons in type i. The fraction of Fe^{3+} is about 50% at the 2H3H state and about 75% at the 2L3H and 2L3L state (Table 1).

REFERENCES

Anderson DL, Bass J (1986) Transition region of the Earth's upper mantle. Nature 320:321-328

Andrault D, Bolfan-Casanova N, Guignot N (2001) Equation of state of lower mantle (Al,Fe)-$MgSiO_3$ perovskite. Earth and Planetary Science Letters 193:501-508

Badro J, Rueff J-P, Vanko G, Monaco G, Fiquet G, Guyot F (2004) Electronic transitions in perovskite: Possible nonconvecting layers in the lower mantle. Science 305:383-386

Bancroft GM (1973) Mössbauer spectroscopy, vol. Halsted Press, John Wiley and Sons, Inc., New York, p 252

Burns RG (1993) Mineralogical Applications of Crystal Field Theory, vol. Cambridge University Press, Cambridge, p 551

Burns RG, Solberg TC (1990) ^{57}Fe-bearing oxide, silicate, and aluminosilicate minerals. In: Coyne LM, S MSW, Blake DF (eds) Spectroscopic characterization of minerals and their surfaces, vol 415. American Chemical Society, Washington DC, pp 262-283

Champion AR, Vaughan RW, Drickamer HG (1967) Effect of pressure on the Mössbauer Resonance in ionic compounds of iron. J. Chem. Phys. 47:2583-2590

Eng PJ, Newille M, Rivers ML, Sutton SR (1998) Dynamically figured Kirkpatrick Baez x-ray microfocusing optics. SPIE Proc. 3449:145

Fei Y, Virgo D, Mysen BO, Wang Y, Mao H-K (1994) Temperature-dependent electron delocalization in (Mg,Fe)SiO_3 perovskite. Am. Mineral. 79:826-837

Fei Y, Zhang L, Corgne A, Watson HC, Shen G, Prakapenka V (2005) Spin transition in (Mg,Fe)O at high pressure. Eos Trans. AGU 86(52) Fall Meet. Suppl., Abstract

Fiquet G, Dewaele A, Andrault D, Kunz M, Le Bihan T (2000) Thermoelastic properties and crystal structure of $MgSiO_3$ perovskite at lower mantle pressure and temperature conditions. Geophysical Research Letters 27(1):21-24

Frost DJ, Langenhorst F (2002) The effect of Al_2O_3 on Fe-Mg partitioning between magnesiowüstite and magnesium silicate perovskite. Earth and Planetary Science Letters 199(1-2):227-241

Frost DJ, Liebske C, Langenhorst F, McCammon CA, Tronnes RG, Rubie DC (2004) Experimental evidence for the existence of iron-rich metal in the Earth's lower mantle. Nature 428:409-412

Hirsch LM, Shankland TJ (1991) Point defects in (Mg,Fe)SiO_3 perovskite. Geophysical Research Letters 18:1305-1308

Ito E, Kubo A, Katsura T, Akaogi M, Fujita T (1998) High-pressure transformation of pyrope $Mg_3Al_2Si_3O_{12}$ in a sintered diamond cubic anvil assembly. Geophysical Research Letters 25(6):821-824

Jackson JM, Sturhahn W, Shen G, Zhao J, Hu MY, Errandonea D, Bass JD, Fei Y (2005) A synchrotron Mossbauer spectroscopy study of (Mg,Fe)SiO_3 perovskite up to 120 GPa. American Mineralogist 90:199-205

Jackson WE, Knittle E, Jr. BGE, Jeanloz R (1987) Partitioning of Fe within high-pressure silicate perovskite: Evidence for unusual geochemistry in the lower mantle. Geophysical Research Letters 14:224-226

Jeanloz R, O'Neill B, Pasternak MP, Taylor RD, Bohlen SR (1992) Mössbauer spectroscopy of $Mg_{0.9}Fe_{0.1}SiO_3$ perovskite. Geophysical Research Letters 19:2135-2138

Jephcoat AP, Hriljac JA, McCammon CA, O'Neill HStC, Rubie DC, Finger LW (1999) High-resolution synchrotron X-ray powder diffraction and Rietveld structure refinement of two $(Mg_{0.95},Fe_{0.05})SiO_3$ perovskite samples synthesized under different oxygen fugacity conditions. American Mineralogist 84:214-220

Katsura T, Sato K, Ito E (1998) Electrical conductivity of silicate perovskite at lower-mantle conditions. Nature 395:493-495

Keppler H, McCammon CA, Rubie DC (1994) Crystal-field charge-transfer spectra of (Mg,Fe)SiO_3 perovskite. American Mineralogist 79:1215-11218

Lauterbach S, McCammon CA, van Aken PA, Langenhorst F, Seifert F (2000) Mössbauer and ELNES spectroscopy of (Mg,Fe)(Si,Al)O_3 perovskite: a highly oxidised component of the lower mantle. Contributions to Mineralogy and Petrology 138:17-26

Li J, Struzhkin VV, Mao H-K, Shu J, Hemley RJ, Fei Y, Mysen B, Dera P, Prakapenka V, Shen G (2004) Electronic spin state of iron in lower mantle perovskite. Proceedings of National Academy of Science 101(39):14027-14030

Li L, Brodholt JP, Stackhouse S, Weidner DJ, Alfredsson M, Price GD (2005) Electronic spin state of ferric iron in Al-bearing perovskite in the lower mantle. Geophysical Research Letters 32(L17307):doi:10.1029/2005/GL023045

Li X, Ming L-c, Manghnani MH, Wang Y, Jeanloz R (1993) Pressure dependence of the electrical conductivity of $(Mg_{0.9}Fe_{0.1})SiO_3$ perovskite. Journal of Geophysical Research 98(B1):501-508

Lin J-F, Struzhkin VV, Jacobsen SD, Hu MY, Chow P, Kung J, Liu H, Mao H-K, Hemley RJ (2005) Spin transition of iron in magnesiowüstite in the Earth's lower mantle. Nature 436:377-380

Liu L-G (1974) Silicate perovskite from phase transformations of pyrope-garnet at high-pressure and high-temperature. Geophysical Research Letters 1:277-280

Mao H-K, Hemley RJ, Fei Y, Shu J, Chen L, Jephcoat AP, Wu Y, Bassett WA (1991) Effect of pressure, temperature, and composition on lattice parameters and density of (Fe,Mg)SiO_3-perovskites to 30 GPa. J. Geophys. Res. 96:8069-8079

Mao H-K, Xu J, Bell PM (1986) Calibration of the ruby pressure gauge to 800 kbar under quasihydrostatic conditions. J. Geophys. Res. 91(B5):4673-4676

Mao HK, Xu J, Struzhkin VV, Shu J, Hemley RJ, Sturhahn W, Hu MY, Alp EE, Vocadlo L, Alfé D, Price GD, Gillan MJ, Schwoerer-Bohning M, Hausermann D, Eng P, Shen G, Giefers H, Lübbers R, Wortmann G (2001) Phonon density of states of iron up to 153 gigapascals. Science 292(5518):914-916

McCammon C (1997) Perovskite as a possible sink for ferric iron in the lower mantle. Nature 387:694-696

McCammon C, A., Lauterbach S, Seifert F, Langenhorst F, van Aken PA (2004) Iron oxidation state in lower mantle mineral assemblages I: Empirical relations derived from high-pressure experiments. Earth and Planetary Science Letters 222:435-449

McCammon CA (1998) The crystal chemistry of ferric iron in $Fe_{0.05}Mg_{0.95}SiO_3$ perovskite as determined by Mössbauer spectroscopy in the temperature range 80-293 K. Physics and Chemistry of Minerals 25:292-300

McCammon CA, Rubie DC, Ross II CR, Seifert F, O'Neill HStC (1992) Mössbauer spectra of $^{57}Fe_{0.05}Mg_{0.95}SiO_3$ perovskite at 80 and 198 K. American Mineralogist 77:894-897

Nafziger RH, Ulmer GC, Woermann E (1971) Gaseous buffering for the control of oxygen fugacity at one atmosphere. In: Ulmer GC (ed) Research Techniques for High Pressure and High Temperature, vol 1. Springer-Verlag, New York, pp 9-42

Parise JB, Wang Y, Yeganeh-Haeri Y, Cox DE, Fei Y (1990) Crystal structure and thermal expansion of (Mg,Fe)SiO_3 perovskite. Geophysical Research Letters 17:2089-2092

Pasternak M, Taylor RD, Jeanloz R, Li X, Nguyen JH, McCammon CA (1997) High pressure collapse of magnetism in $Fe_{0.94}O$: Mössbauer spectroscopy beyond 100 GPa. Phy. Rev. Lett. 79(25):5046-5049

Pasternak MP, Milner AP, Rozenberg GK, Taylor RD, Jeanloz R (2004) Pressure induced self-oxidation of $Fe(OH)_2$. Physical Review Letters 92(8):085506

Pasternak MP, Rozenberg GK, Machavariani GY, Naaman O, Taylor RD, Jeanloz R (1999) Breakdown of the Mott-Hubbard state in Fe_2O_3: A first-order insulator-metal transition with collapse of magnetism at 50 GPa. Physical Review Letters 82(23):4663-4666

Richmond NC, Brodholt JP (1998) Calculated role of aluminum in the incorporation of ferric iron into magnesium silicate perovskite. American Mineralogist 83(9-10):947-951

Rueff JP, Krisch M, Cai YQ, Kaprolat A, Hanfland M, Lorenzen M, Masciovecchio C, Verbeni R, Sette F (1999) Magnetic and structural alpha-epsilon phase transition in Fe monitored by X-ray emission spectroscopy. Physical Review B 60:14510-14512

Shannon RD, Prewitt CT (1969) Effective ionic radii in oxides and fluorides. Acta. Crystallogr. Sect. B25:925-946

Shen G, Fei Y, Hålenius U, Y. W (1994) Optical absorption spectra of $(Mg,Fe)SiO_3$ perovskites. Physics and Chemistry of Minerals 20:478-482

Sherman DM (1988) High-spin to low-spin transition of iron(II) oxides at high pressures: Possible effects on the physics and chemistry of the lower mantle. In: Ghose S, Coey JMD, Salje E (eds) Structural and Magnetic Phase Transitions in Minerals, vol 7. Springer-Verlag, New York, pp 113-128

Speziale S, Milner A, Lee VE, Clark SM, Pasternak M, Jeanloz R (2005) Iron spin transition in Earth's mantle. Proceedings of National Academy of Science 102(50):17918-17922

Struzhkin VV, Hemley RJ, Mao HK, Timofeev YA, Eremets MI (2000) Electronic and magnetic studies of materials to megabar pressures. Hyperfine Interactions 128:323-343

Sturhahn W (2000) CONUSS and PHOENIX: Evaluation of nuclear resonant scattering data. Hyperfine Int. 125:149-172

Sturhahn W (2004) Nuclear resonant spectroscopy. Journal of Physics: Condensed Matter 16:S497-S530

Sturhahn W, Gerdau E (1994) Evaluation of time-differential measurements of nuclear-resonance scattering of x-rays. Phys. Rev. B 49(14):9285

Sturhahn W, Jackson JM, Lin J-F (2005) The spin state of iron in minerals of Earth's lower mantle. Geophysical Research Letters 32(L12307):doi:10.1029/2005GL022802

Toellner TS (2000) Monochromatization of synchrotron radiation for nuclear resonant scattering experiments. Hyperfine Int. 113:47-58

Tsutsumi K, Nakamori H, Ichikawa K (1976) X-ray Mn Kb emission spectra of manganese oxides and manganates. Physical Review B 13(2):929-933

Vanpeteghem CB, Angel RJ, Ross NL, Ohtani E, Litasov K (2005) The variation of the crystal structure of magnesium silicate perovskite with chemical composition. Eos Trans. AGU 85(47):Fall Meet. Suppl., MR11A-0910

Wertheim GK (1964) Mössbauer Effect: Principles and Applications, vol. Academic Press, New York

Wood BJ, Rubie DC (1996) The effect of alumina on phase transformations at the 660-kilometer discontinuity from Fe-Mg partitioning experiments. Science 273:1522-1524

Xu J, McCammon C, Poe BT (1998) The effect of alumina on the electrical conductivity of silicate perovskite. Science 282:922-924

Zha CS, Mao HK, Hemley RJ (2000) Elasticity of MgO and a primary pressure scale to 55 GPa. Proc. Natl. Acad. Sci. 97(25):13494-13499

Zhang L, Stanek J, Hafner SS, Ahsbahs H, Grünsteudel HF, Metge J, Rüffer R (1999) ^{57}Fe nuclear forward scattering of synchrotron radiation in hedenbergite $CaFeSi_2O_6$ at hydrostatic pressures up to 68 GPa. American Mineralogist 84:447-453